

# A fundamental plane of galaxy assembly and chemical enrichment within the first 700 Myr after the Big Bang

Kasper E. Heintz<sup>1,2</sup>, Gabriel B. Brammer<sup>1,2</sup>, Clara Giménez-Arteaga<sup>1,2</sup>, Claudia del P. Lagos<sup>3,4,1</sup>, Aswin P. Vijayan<sup>1,5</sup>, Jorryt Matthee<sup>6</sup>, Darach Watson<sup>1,2</sup>, Charlotte A. Mason<sup>1,2</sup>, Anne Hutter<sup>1,2</sup>, Sune Toft<sup>1,2</sup>, Johan P. U. Fynbo<sup>1,2</sup>, Pascal A. Oesch<sup>7,1,2</sup> and Victoria B. Strait<sup>1,2</sup>

<sup>1</sup>Cosmic Dawn Center (DAWN), Denmark.

<sup>2</sup>Niels Bohr Institute, University of Copenhagen, Jagtvej 128, DK-2200 Copenhagen N, Denmark.

<sup>3</sup>International Centre for Radio Astronomy Research (ICRAR), M468, University of Western Australia, 35 Stirling Hwy, Crawley, WA 6009, Australia.

<sup>4</sup>ARC of Excellence for All Sky Astrophysics in 3 Dimensions (ASTRO 3D).

<sup>5</sup>DTU-Space, Technical University of Denmark, Elektrovej 327, 2800, Kgs. Lyngby, Denmark.

<sup>6</sup>Department of Physics, ETH Zürich, Wolfgang-Pauli-Strasse 27, Zürich, 8093, Switzerland.

<sup>7</sup>Observatoire de Genève, Université de Genève, Chemin Pegasi 51, CH-1290 Versoix, Switzerland.

## Abstract

Galaxies throughout the last 12 Gyr of cosmic time follow a single, universal fundamental plane that relates their star-formation rates (SFRs), stellar masses ( $M_*$ ) and chemical abundances [1, 2]. Deviation from these fundamental scaling relations would imply a drastic change in the processes that regulate galaxy evolution. Observations have hinted at the possibility that this relation may be broken in the very early universe [1, 3, 4]. However, until recently, chemical abundances of galaxies could be only measured reliably as far back as redshift  $z = 3.3$  [5, 6]. With JWST, we can now characterize

the SFR,  $M_*$ , and gas-phase metallicity of galaxies during the first few hundred million years after the Big Bang, at redshifts  $z \approx 7 - 10$ . Here we show that galaxies at this epoch follow universal SFR- $M_*$ -main-sequence and mass-metallicity scaling relations, but their chemical abundance is a factor of three lower than expected from the fundamental plane of later galaxies. Compared to state-of-the-art simulations [7–9], these findings suggest a more rapid onset of galaxy assembly and star formation than previously anticipated, and further indicate that galaxies at this time are still intimately connected with the intergalactic medium and subject to continuous infall of pristine gas which effectively dilutes their metal abundances.

## Main text

We identified the galaxies through a blind and uniform selection of targets from recently-obtained public datasets with JWST Near-Infrared Spectrograph (NIRSpec) prism spectroscopy of the gravitational lensing clusters Abell 2744 (JWST DD-2756, PI: Chen) and RXJ-2129 (JWST DD-2767, PI: Kelly). We included all galaxies for which at least the nebular emission lines [O III]  $\lambda 4959, 5007$  were detected, requiring  $S/N \gtrsim 3$  per wavelength element in the spectral regions covering the lines. These fields also have extensive photometric coverage with the JWST Near Infrared Camera (NIRCam). The spectroscopic and photometric data were obtained from the MAST archive and reduced using `grizli` and custom-made pipelines (see Methods). We identify six targets matching these criteria at  $z \gtrsim 7$ , i.e. within the first 700 Myr after the Big Bang, as summarized in Table 1. Throughout the paper we assume the concordance  $\Lambda$ CDM cosmology [10].

We scale the optimally-extracted 1D spectra to match the photometry for each source to improve the absolute flux calibration and correct for potential slitlosses, typically finding absolute corrections of 1.6–1.8. Specifically, we create synthetic spectra based on the best-fit continuum and emission line models (see Methods) and integrate the observed flux over the entire NIRCam passbands with similar wavelength coverage (typically F277W, F356W, and F444W). These cover a significant fraction of the rest-frame optical continuum, redshifted to  $\approx 2 - 5\mu\text{m}$ , and the most prominent nebular emission lines,  $H\beta$  and [O III]  $\lambda 4959, 5007$ . The final photometrically-calibrated spectra used throughout the main analysis are shown in Fig. 1.

We determine the spectroscopic redshift of each galaxy by fitting a continuum model with Gaussian line profiles of the most prominent nebular emission line imposed on to each spectrum. The redshifts span  $z_{\text{spec}} = 7.87 - 9.51$ , corresponding to 500 – 650 Myr after the Big Bang. The individual redshifts are summarized in Table 1, and marked for each source in Fig. 1. We measure the line fluxes from the Gaussian line profiles modelled in the photometrically-calibrated spectra. In all cases we detect the [O III]  $\lambda 4959, 5007$  doublet, and in the majority of cases the Balmer lines  $H\beta$  and  $H\gamma$ , as well as the [O II]  $\lambda 3726, 3729$  doublet. The [O II] doublet is, however, not resolved in our spectra so we therefore only consider the sum of the doublet transitions. We are also not able to resolve the auroral [O III] 4363 line transition from  $H\gamma$ , except for the galaxy at  $z = 9.501$  (see Methods and ref [11]). This feature will generally be resolved with the NIRSpec prism only for the highest redshift sources, where the line transition is located in the redder, higher wavelength-resolution region.

We model the spectral energy distribution (SED) of each galaxy using the Bayesian Analysis of Galaxies for Physical Inference and Parameter ESTimation (BAGPIPES) software package [12]. We infer the physical properties of each source based on the NIRCcam photometry (Methods). We assume a simple constant star-formation history (SFH) and correct the constraints by the magnification factors due to lensing. We infer stellar masses in the range  $M_{\star} = 10^{7.2} - 10^{8.6} M_{\odot}$ , as summarized in Table 1, and ages from 3 Myr (for Abell-z7885) up to  $\approx 50$  Myr (for RXJ-z814). We tested various prescriptions for the SFH and attenuation curves and found that they were overall consistent, independent of the exact parametrizations used (see Methods). Since the derived stellar masses can have large uncertainties depending on the exact underlying SFH [13, 14], however, we apply an additional 0.5 dex systematic uncertainty to the statistical errors in the following analysis.

We measure the Balmer decrement,  $H\beta/H\gamma$ , for each galaxy and find that they are all consistent with the theoretically predicted intrinsic ratio from the Case B recombination scenario, implying low dust contents. We infer the star-formation rate (SFR) for each galaxy based on the  $H\beta$  flux measurements derived from the re-scaled spectra as

$$\text{SFR}_{H\beta}(M_{\odot}/\text{yr}) = 5.5 \times 10^{-42} L_{H\beta}(\text{erg/s}) \times f_{H\alpha/H\beta}, \quad (1)$$

assuming a Kroupa initial mass function (IMF) [15] and the theoretical  $f_{H\alpha/H\beta} = 2.76$  ratio from the Case B recombination model at  $T_e = 2 \times 10^4$  K.

We derive a range of  $\text{SFR}_{\text{H}\beta} = 2 - 15 M_{\odot} \text{yr}^{-1}$  based on the photometrically-calibrated spectra and taking into account the relevant magnification factors. The statistical uncertainties from the  $\text{H}\beta$  line flux measurements are typically 10 – 20%, whereas the uncertainties from the choice of the IMF is  $\approx 20 - 30\%$ . We therefore conservatively assume a 0.4 dex total uncertainty for each SFR measurement as summarized in Table 1. Combined with the stellar masses inferred from the photometry, we find that the identified galaxies at  $z \sim 7 - 10$  all seem to follow the same  $\text{SFR}-M_{\star}$  “main-sequence”, quantified by  $\log(\text{SFR}/M_{\odot} \text{yr}^{-1}) = 0.5 \times \log(M_{\star}/M_{\odot}) - 3.3$  with a scatter of 0.3 dex. This is substantially higher by  $5\sigma$  than the observed local, main-sequence of star-forming galaxies at  $z \approx 0$ , but only marginally (i.e. within  $1\sigma$ ) higher than the  $z = 4$  main-sequence [16].

Since we are, in most cases, not able to resolve or securely constrain the auroral  $[\text{O III}] \lambda 4363$  line transition, we rely on the strongest nebular emission lines to constrain the gas-phase metallicities from the inferred oxygen abundance,  $12 + \log(\text{O}/\text{H})$ . We adopt the strong-line  $\text{O}_{32}$  calibration derived for local galaxies [2], except for the galaxy RXJ-z950 [11], where we determine the metallicity directly using the  $T_e$ -method [17] (Methods). The  $\text{O}_{32}$  calibration was chosen as being the most robust given the range of ionization parameters and  $[\text{O III}] \lambda 5007/\text{H}\beta$  ratios, and also yielded the most consistent metallicity compared to the direct  $T_e$ -method for RXJ-z950 (Methods).

The mass-metallicity relation of the galaxies at  $z \approx 7 - 10$  are shown in Fig. 2. We observe that they all follow the same approximate log-linear relation, quantified as  $12 + \log(\text{O}/\text{H}) = 0.3 \times \log(M_{\star}/M_{\odot}) + 5.15$ , with a 0.15 dex scatter. We also compare our observations to the three galaxies at  $z \gtrsim 7$  identified in the Early Science Observations (ERO), with properties from [18]. Including the mass-metallicity relations of strong  $[\text{O III}]$ -emitting galaxies at  $z \approx 5 - 7$  in different mass bins [19], reveal no strong evolution from  $z \approx 6$  to  $z = 8$ . We do not observe any evidence for a high-mass flattening as observed for local galaxies around  $M_{\star} \approx 10^{10} M_{\odot}$  [6], either because we do not reach equally high stellar masses, or simply due to small-number statistics from the still limited galaxy sample. The galaxies at  $z \approx 7 - 10$  show substantially lower gas-phase metallicities by  $5\sigma$  than local star-forming galaxies at  $z \approx 0$  at equivalent stellar masses [6]. At redshifts  $z \approx 3.3$ , which was previously the most distant redshifts where metallicities could be robustly estimated due to the limited ground-based NIR coverage, we also observe systematically lower gas-phase metallicities by 0.25 dex though only at the  $2\sigma$  level.

We compare our observations of galaxies at  $z \approx 7 - 10$  to the recent cosmological simulations: *Astraeus* [8, 9] and the Feedback in Realistic Environment (FIRE) [7], extrapolated to  $z = 8$ , in Fig. 2. We also considered the First Light and Reionisation Epoch Simulations (FLARES) [20, 21] and the TNG-50 simulations [22, 23], but since they overall show non-evolving metallicities from the locally observed  $z \sim 0$  mass-metallicity relation ([21], and see Methods) we do not consider them representative for the high- $z$  galaxy populations. Our observations can, however, now effectively be used to constrain the stellar and chemical build-up in these various simulations. The observed mass-metallicity relation at  $z \approx 7 - 10$  systematically reveals more chemically evolved galaxies at a given stellar mass than predicted from simulations, while the slopes are otherwise generally consistent. This could indicate a more evolved stellar population and overall more rapid galaxy build-up and assembly than previously expected, in line with recent complementary JWST observations revealing massive, early galaxies [24–26]. Assuming a core-collapse supernova yield of  $0.015 M_{\odot}$  oxygen per solar mass of stars formed [27], these early galaxies have already created  $10^5 - 5 \times 10^7 M_{\odot}$  of oxygen. Assuming that the majority of the oxygen is still in the gas-phase, this implies gas masses of  $M_{\text{gas}} = 10^{9.5} - 10^{10.5} M_{\odot}$  based on the inferred metallicities. These excessive gas reservoirs are consistent with estimates using the bright ISM cooling line [C II]– $158\mu\text{m}$  from galaxies at  $z \approx 6 - 8$  as a gas tracer [28].

We further test whether these early metal-enriched galaxies follow the same fundamental mass-metallicity-SFR relation (FMR) observed for galaxies within the last 12 Gyr, i.e. from redshifts  $z = 0 - 3$  [1, 2]. Fig. 3 shows the metallicity offsets from the local FMR based on the inferred SFR and  $M_{\star}$  for each of the galaxies at  $z \approx 7 - 10$ . We observe systematically lower  $Z_{\text{obs}}$  than  $Z_{\text{FMR}}$ , with a weighted mean and standard deviation of  $Z_{\text{obs}} - Z_{\text{FMR}} = -0.46 \pm 0.07$  for the primary sample galaxies at  $z \sim 7 - 10$ . This offset seems to already be in place by  $z \approx 5 - 7$ , as revealed by the comparable observations of [O III]-emitters in different mass bins [19]. Comparing to the redshift-dependent 4D fundamental relation predicted from simulations [9], we overall find higher metallicities than predicted (Methods), commensurate with the more chemically evolved mass-metallicity relation. There have already been some early results hinting that local FMR relation may not hold at  $z \gtrsim 3.5$  [1, 3, 4]. Most of these observations relied on limited samples sizes, and the majority of sources were highly star-forming systems, making them overall unrepresentative of the typical galaxy population at the respective redshifts. The first JWST study of the three galaxies at  $z \gtrsim 7$  observed as part of the ERO was

also inconclusive [18]. The results presented here are thus the first to robustly verify this offset and divergence from the local FMR at early cosmic times based on a statistically significant sample.

The drastic drop in metallicity in these early universe galaxies could be explained by significant accretion from the intergalactic medium that rapidly replenishes the galaxies with continuous infall of neutral, pristine gas. This process effectively dilutes the metals, reducing the overall chemical abundance [29]. Gas accretion from the intergalactic medium is expected theoretically to be an important process for feeding star-forming galaxies in the first  $\approx 1\text{--}2$  Gyr of cosmic time [30, 31]. Recent observations of abundant gas reservoirs at high-redshift [28, 32] support this hypothesis. In this scenario, it is the exhaustion of these reservoirs that is responsible for the peak and rapid drop in the cosmic star-formation rate observed at redshift  $z \approx 1\text{--}3$  [33, 34].

**Table 1** Physical properties of the primary sample galaxies at  $z \approx 7 - 10$ .

Galaxy ID	$z_{\text{spec}}$	$\text{SFR}_{\text{H}\beta}/M_{\odot}\text{yr}^{-1}$	$\log(M_{\star}/M_{\odot})$	$12 + \log(\text{O}/\text{H})_{\text{O}32}$	$\mu$
RXJ-z950	9.5008	$1.7^{+2.6}_{-1.0}$	$8.47^{+0.15}_{-0.18}$	$7.32^{+0.10}_{-0.12}$	$19.2 \pm 3.6$
RXJ-z814	8.1496	$3.2^{+4.9}_{-1.9}$	$7.86^{+0.28}_{-0.34}$	$> 7.34$	$2.25 \pm 0.14$
RXJ-z815	8.1523	$8.7^{+13.2}_{-5.2}$	$7.88^{+0.07}_{-0.05}$	$7.56^{+0.16}_{-0.25}$	$1.46 \pm 0.03$
Abell-z7878	7.8783	$< 12.5$	$8.74^{+0.07}_{-0.06}$	$8.19^{+0.19}_{-0.33}$	$1.33 \pm 0.04$
Abell-z7885	7.8854	$4.2^{+6.3}_{-2.5}$	$7.98^{+0.03}_{-0.02}$	$7.34^{+0.11}_{-0.14}$	$2.12 \pm 0.06$
Abell-z7874	7.8739	$13.5^{+20.4}_{-8.1}$	$8.71^{+0.07}_{-0.07}$	$7.65^{+0.23}_{-0.50}$	$1.41 \pm 0.04$

Note. The listed properties are not corrected for the magnification factor provided in Col. 6.

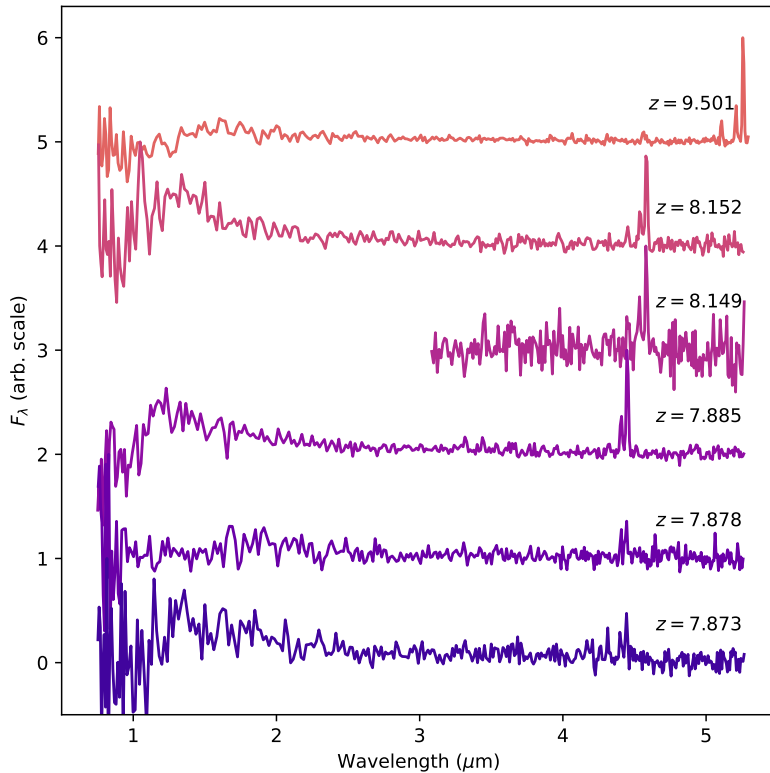


**Fig. 1** JWST/prism spectra of the six primary targets analyzed in this work. The spectroscopic redshifts are marked for each galaxy, ranging from  $z_{\text{spec}} = 7.873$  (bottom) to  $z_{\text{spec}} = 9.501$  (top).



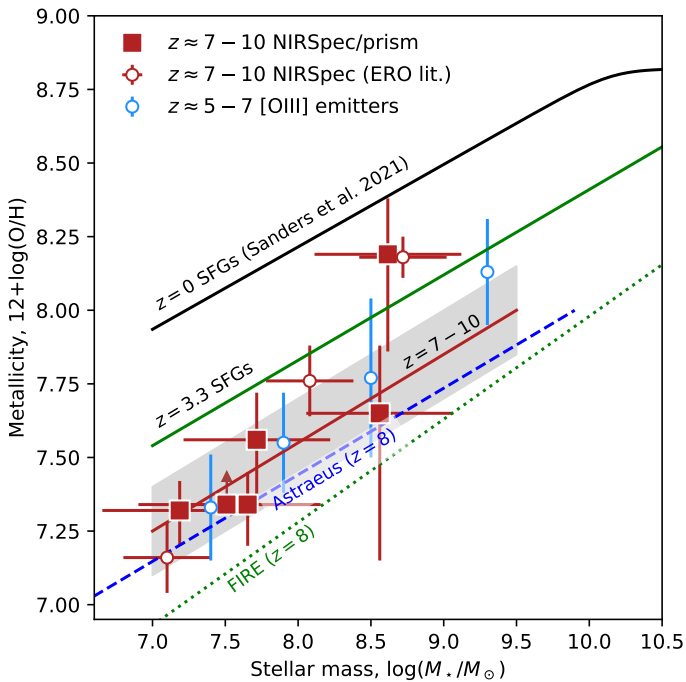


**Fig. 2** The stellar mass-metallicity relation of galaxies at  $z \sim 7-10$ . Red filled squares marked the primary sources analyzed in this work where the errorbars represent the combined statistical and systematic uncertainties. The open red circles show literature JWST/NIRSpec ERO data of three additional galaxies at  $z \gtrsim 7$  [18] and the open blue circles represent the results from [O III]-emitters at  $z \sim 5-7$  in different mass bins [19]. The black (green) solid line marks the mass-metallicity relation of star-forming galaxies at  $z = 0$  ( $z = 3.3$ ) derived from the literature [6]. The blue-dashed and green-dotted lines represent mass-metallicity relation predictions from simulations [7, 9], extrapolated to  $z = 8$ .

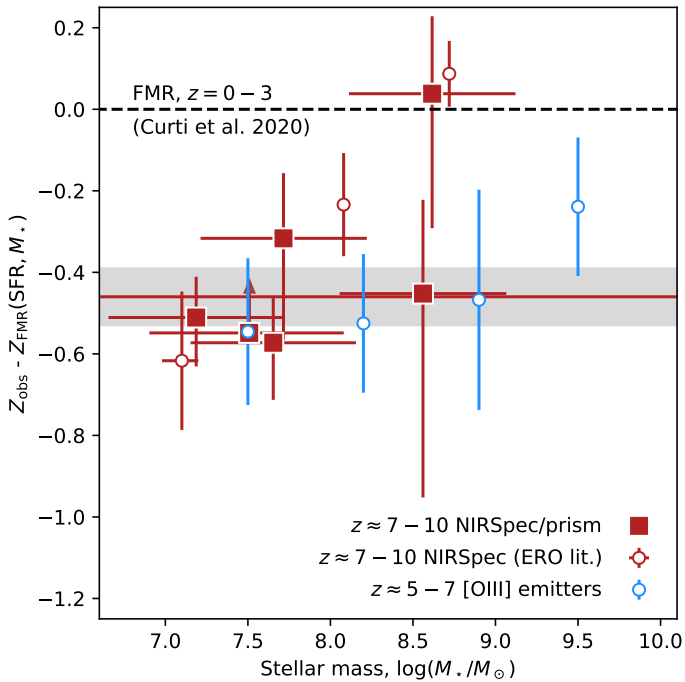


**Fig. 3** Offset from the fundamental-plane metallicity relation (FMR) at  $z = 0 - 3$  [2]. Symbol notation follow Fig. 2. The red solid line and grey-shaded region represent the weighted mean and standard deviation of the offset for the primary sample of galaxies at  $z \sim 7 - 10$ . The majority of galaxies at both  $z \approx 5 - 7$  and  $z \approx 7 - 10$  show lower metallicities than predicted from the local FMR based on their SFRs and stellar masses.

**Acknowledgments.** We are grateful that the GLASS and UNCOVER collaborations made their early data publicly available. K.E.H. acknowledges support from the Carlsberg Foundation Reintegration Fellowship Grant CF21-0103. C.A.M and A.H. acknowledge support by the VILLUM FONDEN under grant 37459. The Cosmic Dawn Center (DAWN) is funded by the Danish National Research Foundation under grant No. 140. This work is based on observations made with the NASA/ESA/CSA James Webb Space Telescope. The data were obtained from the Mikulski Archive for Space Telescopes at the Space Telescope Science Institute, which is operated by the Association of Universities for Research in Astronomy, Inc., under NASA contract NAS 5-03127 for JWST.

**Author contributions.** K.E.H. wrote the manuscript and lead the analysis. G.B. reduced and extracted the photometric and spectroscopic data. C.G.-A. performed the SED modelling. All authors contributed to the manuscript and aided the analysis and interpretation.

**Declarations.** The authors declare no competing financial interests.

**Correspondence.** Correspondence and requests for materials should be addressed to K.E.H. (email: [keheintz@nbi.ku.dk](mailto:keheintz@nbi.ku.dk)).

## Methods

**Cosmology.** Throughout this work we assume concordance, flat  $\Lambda$ CDM cosmology with  $\Omega_m = 0.315$ ,  $\Omega_\Lambda = 0.685$ , and  $H_0 = 67.8 \text{ km s}^{-1} \text{ Mpc}^{-1}$  [10]. We use the cosmology distance calculator from `astropy` [35] to infer the luminosity distances  $D_L$  to the given redshifts.

**Observations and data reduction.** This work is primarily based on the photometric and spectroscopic data taken as part of the public UNCOVER (GO-2561) and GLASS (ERS-1324) surveys, and including observations obtained through the JWST Director’s Discretionary time (DD-2756, PI: Chen and DD-2767, PI: Kelly). The NIRCcam observations were typically taken in six broad-band filters (F115W, F150W, F200W, F277W, F356W, F444W). The photometric data are extracted from the catalog presented by Brammer et al. (in prep), which provides a compilation of the JWST ERO photometric data released to date. The raw data entering this catalog has been reduced using the public software package `grizli` [36], which masks imaging artifacts, provides astrometric calibrations based on the Gaia DR3 catalog, and shifts the images to a common pixel scale of  $0.04''/\text{pixel}$  using `astrodrizzle`. This catalog also includes the most recent updated photometric zero-points, and are all corrected for the Milky Way extinction. We use the aperture-matched photometry derived using a diameter of  $0.5''$  from the catalog.

The 1D spectra are extracted from a custom-made pipeline [37], that utilizes the Stage 2 from the MAST archive. This code performs the standard wavelength, flat-field and photometric calibrations to the individual NIRSpec exposure files<sup>1</sup>. We generate the full combined 2D spectra and optimal [38] 1D extractions with scripts that extend the standard pipeline functionality [37]. We further scale the overall flux densities of the spectra to the derived photometry, matching the integrated flux within the available passbands covering the spectra to improve the absolute flux calibration and take into account potential slitlosses. An example is shown in Fig. 4 for the galaxy RXJ-z815. The required scaling factors are typically of the order  $1.6 - 1.8$ . The NIRSpec prism spectra typically cover the full wavelength range from  $0.7 \mu\text{m}$  to  $5.2 \mu\text{m}$ , and have spectral resolutions ranging from  $\mathcal{R} = 50$  in the blue end to  $\mathcal{R} = 400$  in the red end [39], as presented in Fig. 1.

**Lens models.** To infer the relevant magnification factors for each source, we consider the lens models compiled for the Hubble Frontier fields<sup>2</sup> for the Abel

<sup>1</sup>i.e., calibration levels 1 and 2 with `jwst` version 1.8.2

<sup>2</sup><https://archive.stsci.edu/prepds/frontier/lensmodels/>

2744 cluster. We adopt the GLAFIC-v4 lens model results in this work, but overall find that magnification factors are consistent within 5 – 10% for the various online lens models. For the RXJ-2129 galaxy cluster we adopt the lens model presented by [40]. The magnification factors are summarized in Table 1, typically of the order  $\mu = 1 - 2$  except for the galaxy RXJ-z950 which has  $\mu = 19.2 \pm 3.6$  [11].

**SED modelling.** The SEDs of each galaxy have all been modelled using BAGPIPES [12] to infer their physical properties, in particular their stellar masses. This code uses the stellar population models from Bruzual & Charlot [41]. We fix the redshifts to  $z_{\text{spec}}$  and include nebular emission via CLOUDY [42], allowing the ionization parameter,  $U$ , to vary  $-3 < \log(U) < -1$ , to account for the typically higher ionization parameters at  $z \gtrsim 6$  [43]. We assume the attenuation curve from Salim et al. [44], which better represent low-mass galaxies, allowing the slope ( $\delta$ ) to vary from  $-0.9 < \delta < 0.1$  and the bump strength ( $B$ ) from  $0 < B < 3$ . We assume Gaussian priors on the various dust parameters and infer  $A_V \lesssim 0.1$  mag for all galaxies. We assume a Kroupa 2001 initial mass function (IMF) [15] and set the metallicity to vary between  $0 < Z/Z_{\odot} < 0.5$ . We assume a constant SFH and correct the inferred properties by the magnification factors due to gravitational lensing. For the SFH model, we set the maximum age in a grid from 1 Myr to 500 Myr. Table 1 reports the median and 16th and 84th percentiles from the resulting posterior distributions.

We tried various sets of combinations using different parametrizations of the SFH and dust laws, including a constant and delayed SFH and a Salim [44] vs. Calzetti [45] dust attenuation curve. An exponentially declining SFH is likely not an accurate representation of these very high- $z$  galaxies and may overestimate the inferred stellar masses with increasing SFRs. Assuming a Salim over a Calzetti-like attenuation curve effectively decreases the inferred  $A_V$  due to the steeper functional form of the Salim curve. The slope of the attenuation curve is related to the dust opacity and grain size distribution, which introduces an apparent dependence on the stellar mass as well [44] such that more massive galaxies have shallower slopes. However, we found that our results were remarkably consistent overall (within 0.1 dex in stellar mass estimates), independent of the exact prescriptions used.

**Line flux measurements.** To estimate the line fluxes for each galaxy, we model the continuum of the photometrically-calibrated spectra with a smooth double power law, and impose the most prominent redshifted nebular emission

lines: H $\beta$ , H $\gamma$ , [O III]  $\lambda$ 4959, 5007, and [O II]  $\lambda$ 3727 on this model. The redshift  $z_{\text{spec}}$  and line widths are tied for all the lines, such that only the line fluxes can vary across transitions. The functional form of the continuum model is also allowed to vary freely, since we do not attempt to derive any physical properties from the underlying stellar continuum here. The spectrum and best-fit model is shown for an example galaxy in Fig. 5. The line flux measurements for the primary targets from this work are summarized in Table 2.

**Metallicity calibrations.** In the majority of cases we are not able to resolve the auroral [O III]  $\lambda$ 4363 line transition, which provides a direct measure of the oxygen abundance through the  $T_e$ -method. For these cases we therefore resolved to the  $O_{32}$  strong-line calibration from [2]. This particular calibration was chosen as the only one being able to reproduce the metallicity inferred from the direct  $T_e$ -method for the galaxy RXJ-z950 for which the auroral [O III]  $\lambda$ 4363 line could be resolved, see Fig. 6. Other calibrations such as the  $R_{23}$  and  $O_3\text{H}\beta$  diagnostics inferred for galaxy samples at  $z \approx 0$  [2] and even for local analogs of high-redshift galaxies [46] instead over- or underpredicted the direct  $T_e$ -metallicity by 0.3 - 0.5 dex at 3 - 5 $\sigma$  confidence. This largely seems to be an effect of the observed line ratios being close to the peak of the double-valued polynomials describing these relations, where the  $O_{32}$  calibration provides the most robust constraints for the ionization parameters measured here.

To determine the metallicity based on the direct  $T_e$ -method for the galaxy RXJ-z950, first presented in [11], we follow the iterations outlined by [17] to solve for the oxygen abundance as a function of electron temperature and density. For all  $n_e \lesssim 10^4 \text{ cm}^{-3}$ , we find temperatures  $T_e = (2.4 \pm 0.5) \times 10^4 \text{ K}$  and gas-phase metallicities  $12 + \log(\text{O}/\text{H}) = 7.32^{+0.10}_{-0.12}$ , with the oxygen abundance dominated by the double-ionized O III state. An average electron temperature of  $T_e = 2.2 \times 10^4 \text{ K}$  is also recovered from the stack of [O III]-emitters at  $z \approx 5 - 7$  [19].

For the main analysis we adopt the SFRs, stellar masses and gas-phase metallicities for the galaxies observed as part of the JWST-ERO from the literature [18]. For the galaxy at  $z = 8.496$  we include the results from [47], as they have been derived in a consistent manner to the results presented here.

**Simulations of the mass-metallicity relation at  $z \approx 8$ .** Overall, we find in Fig. 7 that it is only the Astraeus and FIRE simulations that are able to recover the significant offsets from the observed  $z = 0$  to  $z = 3.3$  empirical mass-metallicity relations. The predictions from the TNG-50 simulations

[extracted using the abundance ratios of gas cells weighted by the star formation rate within twice the half mass radius of galaxies; 22, 23] at  $z = 8$  almost directly follow the observed mass-metallicity relation for galaxies at  $z = 0$  [6], which is inconsistent with the overall evolution of the relation, even at  $z < 3$ . Both the FLARES [measured by using the abundance ratios of gas particles weighted by their star formation rate within a 30 pkpc radius from the centre of potential; 20, 21] and FirstLight [48] simulations, when extrapolated to low stellar masses, seem to be marginally consistent with the observed mass-metallicity relation for galaxies at  $z \sim 7 - 10$ . However, the slopes of both curves appear to be significantly steeper than observed, effectively predicting more metal-enriched galaxies at  $M_{\star} \gtrsim 10^8 M_{\odot}$ . It should be noted, however, that both the absolute normalisation and the slope of the mass-metallicity relation are subject to the uncertainties in the metal yields of stars of all masses as well as the stellar feedback models implemented in the different simulations. For this reason, predicting the relative evolution of the mass-metallicity relation with redshift has been the most important so far. With these observations we can now place constraints on the absolute normalization and slope of the mass-metallicity of galaxies out to  $z \approx 10$ , crucial to improve current cosmological simulations modelling the first galaxy populations.

As described in the Main Text, the mass-metallicity relation predicted from the Astraeus simulation at  $z = 8$  [derived from the ratio of the simulated metal and gas mass reservoirs and using the latest metal yields from 49] seem to provide the best match in terms of the slope and a marginally consistent absolute normalization to our observations. In Fig. 8 we compare the 4-dimensional fundamental-plane relation from these simulations [9] to our observations, taking into account the SFR, stellar mass, and redshift, to predict the gas-phase metallicity. Here, we recover a positive offset from the 4D FMR( $Z, \text{SFR}, M_{\star}, z$ ), providing additional evidence that this particular simulation underpredicts the chemical enrichment of these early galaxies. Finally, simulations predict that star-forming galaxies already follow a tight main-sequence in terms of their SFR and stellar mass at  $z = 10$  [50], commensurate with our observations. In the future, these tight constraints on the main-sequence and mass-metallicity relation out to  $z \approx 10$  will help define the FMR at early cosmic times.

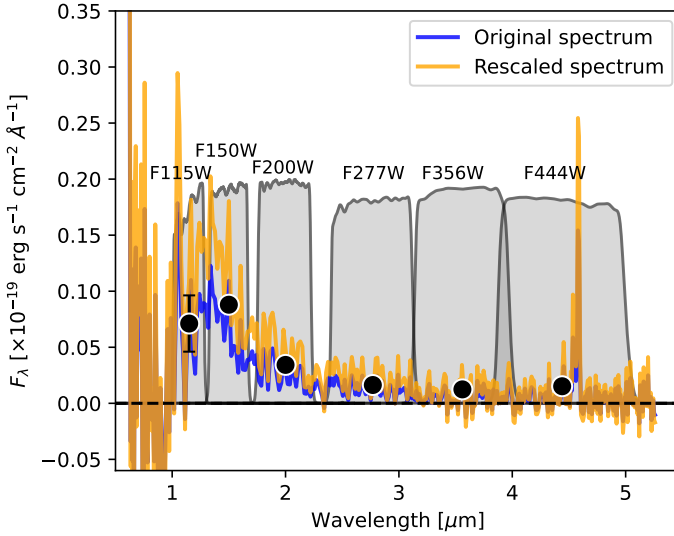


**Fig. 4** The original (blue) and rescaled (orange) 1D spectrum of the galaxy RXJ-z815. The spectrum has been scaled to match the NIRCcam photometry to improve the accuracy of the flux calibration and account for potential slitlosses. The spectrum and photometry have not been corrected for the magnification due to lensing.

**Table 2** Line flux measurements.

Galaxy ID	$z_{\text{spec}}$	$H\beta$	[O III] $\lambda 4960$	[O III] $\lambda 5007$	[O II] $\lambda 3727$
RXJ-z950	9.5008	$17.80 \pm 1.63$	$29.48 \pm 1.66$	$91.53 \pm 1.99$	$5.39 \pm 1.45$
RXJ-z814	8.1496	$5.15 \pm 2.04$	$8.44 \pm 2.02$	$18.41 \pm 2.02$	$< 2.33$
RXJ-z815	8.1523	$9.21 \pm 1.89$	$19.96 \pm 1.92$	$53.28 \pm 2.26$	$2.63 \pm 1.16$
Abell-z7878	7.8783	$< 9.55$	$7.97 \pm 2.88$	$22.56 \pm 4.44$	$8.19 \pm 4.09$
Abell-z7885	7.8854	$6.92 \pm 2.26$	$27.16 \pm 2.31$	$76.73 \pm 2.72$	$9.68 \pm 2.65$
Abell-z7874	7.8739	$15.61 \pm 3.69$	$15.69 \pm 3.64$	$26.84 \pm 4.00$	$5.98 \pm 3.99$

Note. The derived line fluxes are in units of  $10^{19} \text{ erg s}^{-1} \text{ cm}^{-2}$  and have not been corrected for the magnification factor  $\mu$ .



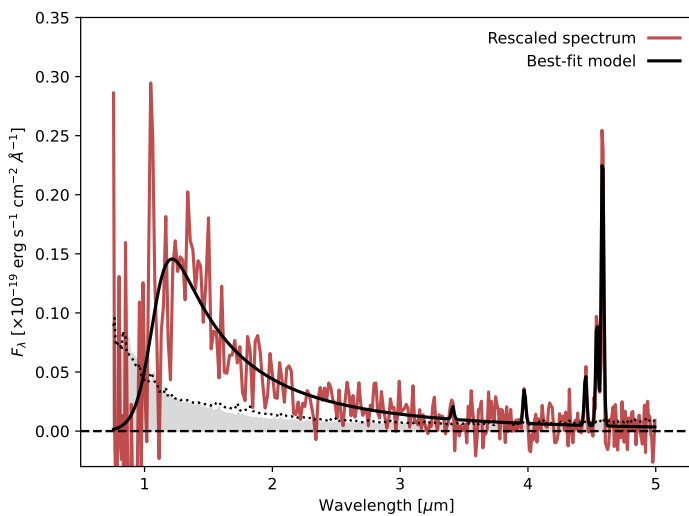


**Fig. 5** The photometrically-calibrated 1D spectrum of the galaxy RXJ-z815 (red), imposed with the best-fit continuum and line emission model (black). The continuum is fit as a smooth double power law, and the emission features are described as Gaussian line profiles tied in redshift and line width.

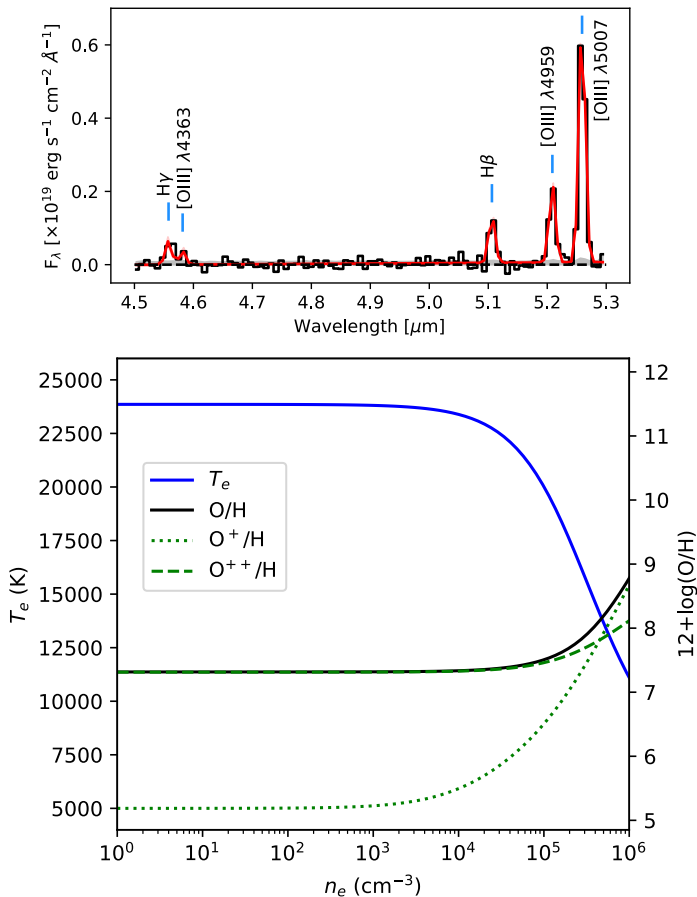


**Fig. 6** (Top): Zoom-in on the photometrically-calibrated 1D spectrum of the galaxy RXJ-z950 (black), marking the most prominent emission line features. The typical strong nebular emission lines are detected, in addition to the auroral [O III]  $\lambda 4363$  transition. The best-fit model of the continuum and line profiles are shown in red. (Bottom): The derived electron temperature  $T_e$  and oxygen abundance  $12+\log(\text{O}/\text{H})$  for RXJ-z950 as a function of electron density  $n_e$ , based on the direct  $T_e$ -method [17].

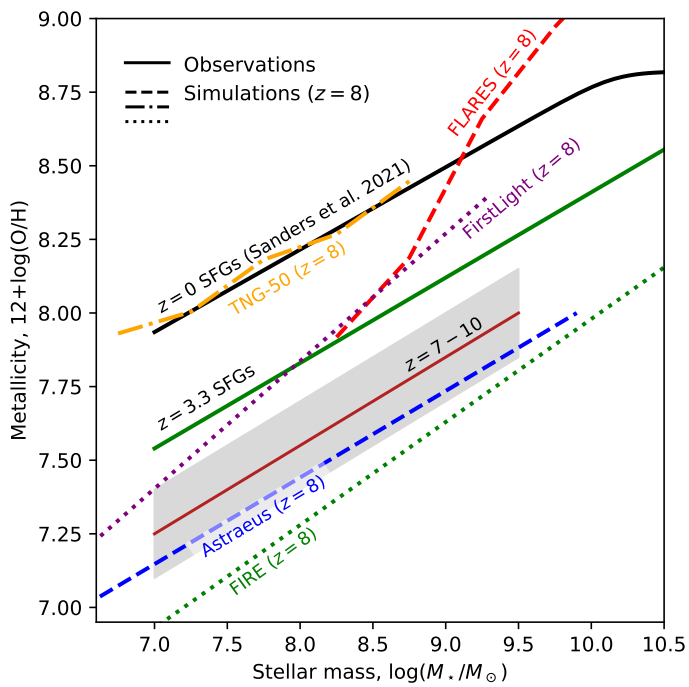


**Fig. 7** Comparison of observed stellar mass-metallicity relations (solid lines) with predictions from a suite of simulations (see text).

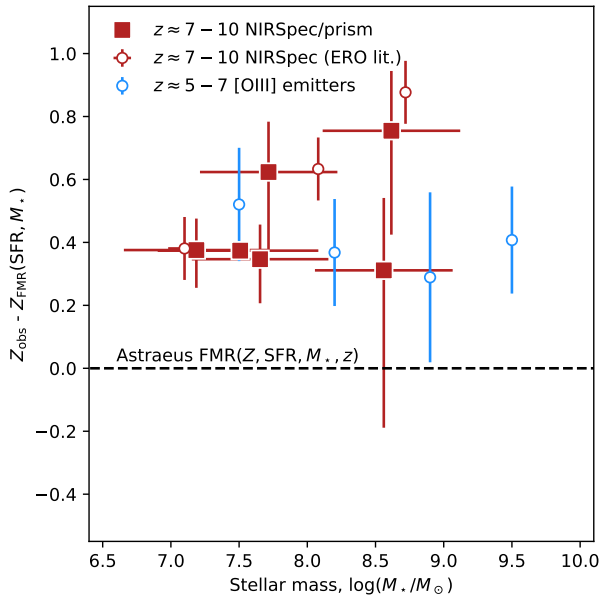


**Fig. 8** Offset from the redshift-dependent fundamental-plane metallicity relation (FMR) from the Astraevs simulations [9]. Symbol notation follow Fig. 2. Galaxies at both  $z \sim 5-7$  and  $z \sim 7-10$ , seem to all be more chemically evolved than predicted from the simulations based on the SFRs and stellar masses.

## References

- [1] Mannucci, F., Cresci, G., Maiolino, R., Marconi, A. & Gnerucci, A. A fundamental relation between mass, star formation rate and metallicity in local and high-redshift galaxies. *Monthly Notices of the Royal Astronomical Society* **408** (4), 2115–2127 (2010). <https://doi.org/10.1111/j.1365-2966.2010.17291.x>, [arXiv:1005.0006](https://arxiv.org/abs/1005.0006) [astro-ph.CO].
- [2] Curti, M., Mannucci, F., Cresci, G. & Maiolino, R. The mass-metallicity and the fundamental metallicity relation revisited on a fully  $T_e$ -based abundance scale for galaxies. *Monthly Notices of the Royal Astronomical Society* **491** (1), 944–964 (2020). <https://doi.org/10.1093/mnras/stz2910>, [arXiv:1910.00597](https://arxiv.org/abs/1910.00597) [astro-ph.GA].
- [3] Troncoso, P. *et al.* Metallicity evolution, metallicity gradients, and gas fractions at  $z \sim 3.4$ . *Astronomy & Astrophysics* **563**, A58 (2014). <https://doi.org/10.1051/0004-6361/201322099>, [arXiv:1311.4576](https://arxiv.org/abs/1311.4576) [astro-ph.CO].
- [4] Onodera, M. *et al.* ISM Excitation and Metallicity of Star-forming Galaxies at  $z \approx 3.3$  from Near-IR Spectroscopy. *Astrophysical Journal* **822** (1), 42 (2016). <https://doi.org/10.3847/0004-637X/822/1/42>, [arXiv:1602.02779](https://arxiv.org/abs/1602.02779) [astro-ph.GA].
- [5] Christensen, L. *et al.* Gravitationally lensed galaxies at  $2 < z < 3.5$ : direct abundance measurements of Ly  $\alpha$  emitters. *Monthly Notices of the Royal Astronomical Society* **427** (3), 1973–1982 (2012). <https://doi.org/10.1111/j.1365-2966.2012.22007.x>, [arXiv:1209.0775](https://arxiv.org/abs/1209.0775) [astro-ph.CO].
- [6] Sanders, R. L. *et al.* The MOSDEF Survey: The Evolution of the Mass-Metallicity Relation from  $z = 0$  to  $z 3.3$ . *Astrophysical Journal* **914** (1), 19 (2021). <https://doi.org/10.3847/1538-4357/abf4c1>, [arXiv:2009.07292](https://arxiv.org/abs/2009.07292) [astro-ph.GA].
- [7] Ma, X. *et al.* The origin and evolution of the galaxy mass-metallicity relation. *Monthly Notices of the Royal Astronomical Society* **456** (2), 2140–2156 (2016). <https://doi.org/10.1093/mnras/stv2659>, [arXiv:1504.02097](https://arxiv.org/abs/1504.02097) [astro-ph.GA].
- [8] Hutter, A. *et al.* Astraeus I: the interplay between galaxy formation and reionization. *Monthly Notices of the Royal Astronomical Society* **503** (3), 3698–3723 (2021). <https://doi.org/10.1093/mnras/stab602>, [arXiv:2004.08401](https://arxiv.org/abs/2004.08401) [astro-ph.GA].
- [9] Ucci, G. *et al.* Astraeus V: The emergence and evolution of metallicity scaling relations during the Epoch of Reionization. *arXiv e-prints* [arXiv:2112.02115](https://arxiv.org/abs/2112.02115) (2021). [arXiv:2112.02115](https://arxiv.org/abs/2112.02115) [astro-ph.GA].

- [10] Planck Collaboration *et al.* Planck 2018 results. VI. Cosmological parameters. *Astronomy & Astrophysics* **641**, A6 (2020). <https://doi.org/10.1051/0004-6361/201833910>, [arXiv:1807.06209](https://arxiv.org/abs/1807.06209) [astro-ph.CO].
- [11] Williams, H. *et al.* Spectroscopy from Lyman alpha to [O III] 5007 of a Triply Imaged Magnified Galaxy at Redshift  $z = 9.5$ . *arXiv e-prints* [arXiv:2210.15699](https://arxiv.org/abs/2210.15699) (2022). [arXiv:2210.15699](https://arxiv.org/abs/2210.15699) [astro-ph.GA].
- [12] Carnall, A. C., McLure, R. J., Dunlop, J. S. & Davé, R. Inferring the star formation histories of massive quiescent galaxies with BAGPIPES: evidence for multiple quenching mechanisms. *Monthly Notices of the Royal Astronomical Society* **480** (4), 4379–4401 (2018). <https://doi.org/10.1093/mnras/sty2169>, [arXiv:1712.04452](https://arxiv.org/abs/1712.04452) [astro-ph.GA].
- [13] Bellstedt, S. *et al.* Galaxy And Mass Assembly (GAMA): a forensic SED reconstruction of the cosmic star formation history and metallicity evolution by galaxy type. *Monthly Notices of the Royal Astronomical Society* **498** (4), 5581–5603 (2020). <https://doi.org/10.1093/mnras/staa2620>, [arXiv:2005.11917](https://arxiv.org/abs/2005.11917) [astro-ph.GA].
- [14] Whitler, L. *et al.* Star formation histories of UV-luminous galaxies at  $z \simeq 6.8$ : implications for stellar mass assembly at early cosmic times. *arXiv e-prints* [arXiv:2206.05315](https://arxiv.org/abs/2206.05315) (2022). [arXiv:2206.05315](https://arxiv.org/abs/2206.05315) [astro-ph.GA].
- [15] Kroupa, P. On the variation of the initial mass function. *Monthly Notices of the Royal Astronomical Society* **322** (2), 231–246 (2001). <https://doi.org/10.1046/j.1365-8711.2001.04022.x>, [arXiv:astro-ph/0009005](https://arxiv.org/abs/astro-ph/0009005) [astro-ph].
- [16] Speagle, J. S., Steinhardt, C. L., Capak, P. L. & Silverman, J. D. A Highly Consistent Framework for the Evolution of the Star-Forming “Main Sequence” from  $z \sim 0$ –6. *Astrophysical Journal Supplement Series* **214** (2), 15 (2014). <https://doi.org/10.1088/0067-0049/214/2/15>, [arXiv:1405.2041](https://arxiv.org/abs/1405.2041) [astro-ph.GA].
- [17] Izotov, Y. I., Stasińska, G., Meynet, G., Guseva, N. G. & Thuan, T. X. The chemical composition of metal-poor emission-line galaxies in the Data Release 3 of the Sloan Digital Sky Survey. *Astronomy & Astrophysics* **448** (3), 955–970 (2006). <https://doi.org/10.1051/0004-6361:20053763>, [arXiv:astro-ph/0511644](https://arxiv.org/abs/astro-ph/0511644) [astro-ph].
- [18] Curti, M. *et al.* The chemical enrichment in the early Universe as probed by JWST via direct metallicity measurements at  $z \sim 8$ . *Monthly Notices of the Royal Astronomical Society* **518** (1), 425–438 (2023). <https://doi.org/10.1093/mnras/stac2737>, [arXiv:2207.12375](https://arxiv.org/abs/2207.12375) [astro-ph.GA].
- [19] Matthee, J. *et al.* EIGER II. first spectroscopic characterisation

- of the young stars and ionised gas associated with strong H $\beta$  and [OIII] line-emission in galaxies at  $z=5-7$  with JWST. *arXiv e-prints* arXiv:2211.08255 (2022). [arXiv:2211.08255](https://arxiv.org/abs/2211.08255) [astro-ph.GA].
- [20] Lovell, C. C. *et al.* First Light And Reionization Epoch Simulations (FLARES) - I. Environmental dependence of high-redshift galaxy evolution. *Monthly Notices of the Royal Astronomical Society* **500** (2), 2127–2145 (2021). <https://doi.org/10.1093/mnras/staa3360>, [arXiv:2004.07283](https://arxiv.org/abs/2004.07283) [astro-ph.GA].
- [21] Vijayan, A. P. *et al.* First Light And Reionization Epoch Simulations (FLARES) - II: The photometric properties of high-redshift galaxies. *Monthly Notices of the Royal Astronomical Society* **501** (3), 3289–3308 (2021). <https://doi.org/10.1093/mnras/staa3715>, [arXiv:2008.06057](https://arxiv.org/abs/2008.06057) [astro-ph.GA].
- [22] Nelson, D. *et al.* First results from the TNG50 simulation: galactic outflows driven by supernovae and black hole feedback. *Monthly Notices of the Royal Astronomical Society* **490** (3), 3234–3261 (2019). <https://doi.org/10.1093/mnras/stz2306>, [arXiv:1902.05554](https://arxiv.org/abs/1902.05554) [astro-ph.GA].
- [23] Pillepich, A. *et al.* First results from the TNG50 simulation: the evolution of stellar and gaseous discs across cosmic time. *Monthly Notices of the Royal Astronomical Society* **490** (3), 3196–3233 (2019). <https://doi.org/10.1093/mnras/stz2338>, [arXiv:1902.05553](https://arxiv.org/abs/1902.05553) [astro-ph.GA].
- [24] Labbe, I. *et al.* A very early onset of massive galaxy formation. *arXiv e-prints* arXiv:2207.12446 (2022). [arXiv:2207.12446](https://arxiv.org/abs/2207.12446) [astro-ph.GA].
- [25] Naidu, R. P. *et al.* Two Remarkably Luminous Galaxy Candidates at  $z \approx 10 - 12$  Revealed by JWST. *Astrophysical Journal Letters* **940** (1), L14 (2022). <https://doi.org/10.3847/2041-8213/ac9b22>, [arXiv:2207.09434](https://arxiv.org/abs/2207.09434) [astro-ph.GA].
- [26] Finkelstein, S. L. *et al.* A Long Time Ago in a Galaxy Far, Far Away: A Candidate  $z \sim 12$  Galaxy in Early JWST CEERS Imaging. *arXiv e-prints* arXiv:2207.12474 (2022). [arXiv:2207.12474](https://arxiv.org/abs/2207.12474) [astro-ph.GA].
- [27] Peebles, M. S. *et al.* A Budget and Accounting of Metals at  $z \sim 0$ : Results from the COS-Halos Survey. *Astrophysical Journal* **786** (1), 54 (2014). <https://doi.org/10.1088/0004-637X/786/1/54>, [arXiv:1310.2253](https://arxiv.org/abs/1310.2253) [astro-ph.CO].
- [28] Heintz, K. E. *et al.* The ALMA REBELS Survey: The Cosmic H I Gas Mass Density in Galaxies at  $z \approx 7$ . *Astrophysical Journal Letters* **934** (2), L27 (2022). <https://doi.org/10.3847/2041-8213/ac8057>, [arXiv:2206.07763](https://arxiv.org/abs/2206.07763) [astro-ph.GA].

- [29] Maiolino, R. & Mannucci, F. De re metallica: the cosmic chemical evolution of galaxies. *Astronomy and Astrophysics Review* **27** (1), 3 (2019). <https://doi.org/10.1007/s00159-018-0112-2>, arXiv:1811.09642 [astro-ph.GA].
- [30] Lagos, C. d. P. *et al.* Shark: introducing an open source, free, and flexible semi-analytic model of galaxy formation. *Monthly Notices of the Royal Astronomical Society* **481** (3), 3573–3603 (2018). <https://doi.org/10.1093/mnras/sty2440>, arXiv:1807.11180 [astro-ph.GA].
- [31] Yates, R. M., Péroux, C. & Nelson, D. Cosmic metal density evolution in neutral gas: insights from observations and cosmological simulations. *Monthly Notices of the Royal Astronomical Society* **508** (3), 3535–3550 (2021). <https://doi.org/10.1093/mnras/stab2837>, arXiv:2109.06888 [astro-ph.GA].
- [32] Walter, F. *et al.* The Evolution of the Baryons Associated with Galaxies Averaged over Cosmic Time and Space. *Astrophysical Journal* **902** (2), 111 (2020). <https://doi.org/10.3847/1538-4357/abb82e>, arXiv:2009.11126 [astro-ph.GA].
- [33] Madau, P. & Dickinson, M. Cosmic Star-Formation History. *Annual Review of Astronomy and Astrophysics* **52**, 415–486 (2014). <https://doi.org/10.1146/annurev-astro-081811-125615>, arXiv:1403.0007 [astro-ph.CO].
- [34] Zavala, J. A. *et al.* The Evolution of the IR Luminosity Function and Dust-obscured Star Formation over the Past 13 Billion Years. *Astrophysical Journal* **909** (2), 165 (2021). <https://doi.org/10.3847/1538-4357/abdb27>, arXiv:2101.04734 [astro-ph.GA].
- [35] Astropy Collaboration *et al.* Astropy: A community Python package for astronomy. *Astronomy & Astrophysics* **558**, A33 (2013). <https://doi.org/10.1051/0004-6361/201322068>, arXiv:1307.6212 [astro-ph.IM].
- [36] Brammer, G. Grizli: Grism redshift and line analysis software. Astrophysics Source Code Library, record ascl:1905.001 (2019). 1905.001.
- [37] Brammer, G. msaexp: NIRSpec analysis tools (2022). URL <https://github.com/gbrammer/msaexp>.
- [38] Horne, K. An optimal extraction algorithm for CCD spectroscopy. *Publications of the Astronomical Society of the Pacific* **98**, 609–617 (1986). <https://doi.org/10.1086/131801> .



- [39] Jakobsen, P. *et al.* The Near-Infrared Spectrograph (NIRSpec) on the James Webb Space Telescope. I. Overview of the instrument and its capabilities. *Astronomy & Astrophysics* **661**, A80 (2022). <https://doi.org/10.1051/0004-6361/202142663>, [arXiv:2202.03305](https://arxiv.org/abs/2202.03305) [astro-ph.IM].
- [40] Zitrin, A. *et al.* Hubble Space Telescope Combined Strong and Weak Lensing Analysis of the CLASH Sample: Mass and Magnification Models and Systematic Uncertainties. *Astrophysical Journal* **801** (1), 44 (2015). <https://doi.org/10.1088/0004-637X/801/1/44>, [arXiv:1411.1414](https://arxiv.org/abs/1411.1414) [astro-ph.CO].
- [41] Bruzual, G. & Charlot, S. Stellar population synthesis at the resolution of 2003. *Monthly Notices of the Royal Astronomical Society* **344** (4), 1000–1028 (2003). <https://doi.org/10.1046/j.1365-8711.2003.06897.x>, [arXiv:astro-ph/0309134](https://arxiv.org/abs/astro-ph/0309134) [astro-ph].
- [42] Ferland, G. J. *et al.* The 2017 Release Cloudy. *Revista Mexicana de Astronomía y Astrofísica* **53**, 385–438 (2017). [arXiv:1705.10877](https://arxiv.org/abs/1705.10877) [astro-ph.GA].
- [43] Sugahara, Y. *et al.* Bridging Optical and Far-infrared Emission-line Diagrams of Galaxies from Local to the Epoch of Reionization: Characteristic High [O III] 88  $\mu\text{m}$ /SFR at  $z \lesssim 6$ . *Astrophysical Journal* **935** (2), 119 (2022). <https://doi.org/10.3847/1538-4357/ac7fed>, [arXiv:2207.05236](https://arxiv.org/abs/2207.05236) [astro-ph.GA].
- [44] Salim, S., Boquien, M. & Lee, J. C. Dust Attenuation Curves in the Local Universe: Demographics and New Laws for Star-forming Galaxies and High-redshift Analogs. *Astrophysical Journal* **859** (1), 11 (2018). <https://doi.org/10.3847/1538-4357/aabf3c>, [arXiv:1804.05850](https://arxiv.org/abs/1804.05850) [astro-ph.GA].
- [45] Calzetti, D. *et al.* The Dust Content and Opacity of Actively Star-forming Galaxies. *Astrophysical Journal* **533** (2), 682–695 (2000). <https://doi.org/10.1086/308692>, [arXiv:astro-ph/9911459](https://arxiv.org/abs/astro-ph/9911459) [astro-ph].
- [46] Bian, F., Kewley, L. J. & Dopita, M. A. “Direct” Gas-phase Metallicity in Local Analogs of High-redshift Galaxies: Empirical Metallicity Calibrations for High-redshift Star-forming Galaxies. *Astrophysical Journal* **859** (2), 175 (2018). <https://doi.org/10.3847/1538-4357/aabd74>, [arXiv:1805.08224](https://arxiv.org/abs/1805.08224) [astro-ph.GA].
- [47] Heintz, K. E., Gimenez-Artega, C. & et, a. The gas and stellar content of a metal-poor galaxy at  $z = 8.5$ . *in prep.* (2022) .
- [48] Langan, I., Ceverino, D. & Finlator, K. Weak evolution of the mass-metallicity relation at cosmic dawn in the FirstLight simulations. *Monthly Notices of the Royal Astronomical Society* **494** (2), 1988–1993 (2020).

<https://doi.org/10.1093/mnras/staa880>, [arXiv:1910.11729](https://arxiv.org/abs/1910.11729) [astro-ph.GA].

- [49] Kobayashi, C., Karakas, A. I. & Lugaro, M. The Origin of Elements from Carbon to Uranium. *Astrophysical Journal* **900** (2), 179 (2020). <https://doi.org/10.3847/1538-4357/abae65>, [arXiv:2008.04660](https://arxiv.org/abs/2008.04660) [astro-ph.GA].
- [50] D'Silva, J. C. J., Lagos, C. D. P., Davies, L. J. M., Lovell, C. C. & Vijayan, A. P. Unveiling the main sequence of galaxies at  $z \geq 5$  with the JWST: predictions from simulations. *Monthly Notices of the Royal Astronomical Society* **518** (1), 456–476 (2023). <https://doi.org/10.1093/mnras/stac2878>, [arXiv:2208.06180](https://arxiv.org/abs/2208.06180) [astro-ph.GA].